Korean J. Chem. Eng., 40(5), 1209-1227 (2023)
DOI: 10.1007/s11814-022-1285-y

pISSN: 0256-1115
eISSN: 1975-7220

Ultrasound spray nozzle atomizer as a chemical reaction medium: Evaluation using Villermaux-Dushman test reaction

Mojdeh Basiri* **and Masoud Rahimi*,**,†**

*Department of Chemical Engineering, Faculty of Engineering, Razi University, Kermanshah, Iran
**Chemical Engineering Advance Research Center, Razi University, Kermanshah, Iran
(*Received 22 July 2022 • Revised 6 September 2022 • Accepted 8 September 2022*)

Abstract−The present work illustrates the po ssibility of atomizing the reactant mixture using a n ultrasound spray nozzle atomizer to increase reactant contact surface area. The more surface area of the mist-like spray generated due to the atomization provides a means for mixing of reactants, thereby enhancing the reaction rate. Therefore, this work implements an ultrasound spray nozzle atomizer as a reactor. The micromixing efficiency of this novel reactor was evaluated using the Villermaux-Dushman test reaction protocol. An inlet micromixer was placed upstream of the ultrasonic atomizer reactor to provide an early mixing of the reactants. Two simple Y-shaped micromixers with diameters of 0.8 mm and 1.5 mm were examined as the inlet micromixers. The effects of flow rate ratio, flow rate, reactant concentration and inlet micromixer diameter on micromixing efficiency were investigated. Furthermore, the micromixing time was calculated based on the incorporation model through a detailed mathematical formulation. For the studied ranges of operating conditions, the micromixing time was in the range of 0.1-1 s. The small value of estimated micromixing times confirmed that the proposed technique is a valuable concept for intensifying micromixing in chemical reactors.

Keywords: Ultrasound, Atomizer, Ultrasonic Nozzle, Atomizer Reactor, Mixing; Villermaux-Dushman Reaction

INTRODUCTION

Mixing is a fundamental unit operation in many industrial fields: pharmaceutical, food, cosmetic, and industries involved with polymers, adhesives, and paintings [1,2]. Effective mixing also has crucial importance on chemical reaction performance where different species must come into contact efficiently. Moreover, all other process parameters, such as heat and mass transfer, operating time and cost, process safety, and product quality, could be affected through the mixing process. In liquid-phase chemical reactions, the conversion a nd selectivity strongly depend on the mixing [3].

Mixing takes place at three different scales, namely, macromixing, mesomixing, and micromixing, as introduced by [4]. Mixing at the molecular level (micromixing) significantly affects a chemical process and its characteristics. This is more important in fast reactions such as precipitation, polymerization, crystallization and combustion reactions [5]. The micromixing effect in these rapid reactions is difficult to isolate from the reaction since the mixing highly depends on the reaction kinetics. Hence, it has been identified as an especially important phenomenon of chemical systems dealing with fast reaction kinetics and consequently affects the final product both quantitatively and qualitatively. If the reaction characteristic time scale is smaller than, or close to, the micromixing time, the mixing must be realized before the reaction is completed [6].

Mixing intensification has been the subject of research in mixing technology and is still developing quickly. To intensify mixing, several different reactors, including stirred tank reactor, tubular reactor, centrifugal pump, jet reactor, Kenics static reactor, microreactor, tee mixers, Couette flow reactor, rotor-stator mixers, aerated stirred tank, static mixer, ultrasound reactor, aerated stirred tank, static mixer, semi-batch reactor, electrohydrodynamic mixer, sliding-surface mixing device, impinging stream reactor, rotating packed bed reactor, have been devised and studied so far [7-9].

Due to the importance of the mixing process, quantitative experimental methods have been developed to characterize and evaluate micromixing performance. Among many different characterization techniques developed over the past years, competing chemical reaction methods are widely used. Reaction selectivity and yield are used to characterize the extent of micromixing performance [10,11]. The Villermaux-Dushman method (iodide-iodate reaction) is the main test reaction commonly applied to investigate micromixing efficiency for new proposed mixing devices and has been implemented in numerous publications by many authors [6,10,12-14].

To intensify micromixing, many researchers have used microreaction technology in laboratory and industrial-scale field applications in recent years. Among the many proposed microstructured devices, micromixers and microchannels have been subjected to much attention, innovations and developme nts in chemical engineering applications [15-17]. Micromixers benefit from short diffusion length between the fluids, high interfacial area, and small internal volumes, which provides high transfer rate capacity, including heat and mass transfer (an improved micromixing efficiency), compared to other conventional types of chemical reactors [17-20]. Hence, the main applications of microchannels are compact heat exchangers, micromixers, and microreactors [15]. In micro-

†To whom correspondence should be addressed.
E-mail: masoudrahimi@yahoo.com; m.rahimi@razi.ac.ir

channel devices, the reduced channel dimensions lead to an increased fluid shear rate, thereby making diffusion the predominant mechanism of mass transfer [1]. Hence, the flow mainly runs in the laminar regime at low Reynolds values. As diffusive mixing (diffusion mechanism) limits the mixing process at the molecular level, the fluid mixing and, thus, the chemical reaction rate run very slowly. The mixing process in the microchannel devices can be performed by convection and diffusion depending on the geometry (channel confluence, twist, bend and obstructions) and the applied operating conditions [14,21,22].

Moreover, atomization can significantly improve the mixing performance of a reactional system since the larger surface area generated by forming droplets will result in better mixing of reactants. Atomization methods are familiar with specific household applications and other applications, e.g., spray painting and spray combustion. Atomization is the process in which the bulk of the liquid is broken down into small droplets conventionally dispersed in a gas known as a spray. Ultrasonic atomization involves the generation of surface waves on the thin liquid film surface flowing over the vibrating surface (atomizing surface) and subsequently breaking up these waves into a fine mist spray (aerosol). Ultrasonic atomizers offer several unique advantages over conventional pneumatic atomizers, making them preferred [23]. As the ultrasonic frequency specifies the droplet size in ultrasonic atomization, it is possible to generate extremely fine droplets along with the excellent ability to control the particle size and very narrow droplet distributions [24-27]. It seems efficient, especially for chemical reaction and mass transfer, since smaller drops can provide a larger surface area per volume and a smaller diffusion length for reactants and mono-sized drops. Mono-sized drops are also desired in a reaction where ultrasonic atomization can establish narrow size distributions [24]. Other ultrasonic atomization characteristics include the simplicity of the process, low working pressure, non-clogging characteristics, and low energy consumption. An added advantage of these atomizers is the lower velocity associated with the atomized droplets as the droplet formation and ejection are decoupled processes. This characteristic is advantageous in particular applications like granulation and coating processes. So far, ultrasonic atomizers have been widely applied in combustion, humidification, spray drying, spray cooling, metallic powder preparation, polymeric microparticle production, and especially in spray coating applications [23,28-30]. To our knowledge, no work has yet been published on ultrasonic atomization of a reaction.

As micromixing is critical in process engineering, developing novel reactors with excellent mixing performance to obtain the desired products is always in demand. In the present work, the micromixing efficiency of an ultrasonic nozzle atomizer is studied. Indeed, the main purpose of this research was to investigate the positive or negative effects of ultrasonic atomization on the mixing quality in a novel reactor. The ultrasonic nozzle atomizer could simultaneously serve as the atomizer, mixer and reactor. The idea behind this research is that by increasing the surface area of reactants through the atomization process, high mixing quality can be achieved. In fact, increasing the surface area of reactants increases the number of collisions. Colliding particles more frequently can intensify mixing. Evaluating the micromixing generated by the ultrasonic atomizer to intensify micromixing and reaction in the atomizer reactor was the main objective of this work. The widely used Villermaux-Dushman protocol was adapted to assess the mixing performance of the reactor quantitatively.

THEORY

1. Theory of Villermaux-Dushman Test Reaction

Several techniques have been employed to evaluate mixing performance. Employing chemical reactions as molecular probes has been invented to characterize the mixing performance [8,14,21]. The competitive parallel iodide-iodate reaction, known as Villermaux-Dushman reaction, was proposed by Fournier et al. [11] and developed by Guichardon and Falk [31] for evaluating micromixing performance. This test reaction is widely used for characterizing mixing in batch, semi-batch mode, and continuous flow micromixers [11,15,31-34].

The present work implemented the successive well-known Villermaux-Dushman test reaction in the ultrasonic nozzle system. This test reaction makes it possible to quantify the micromixing spectrophotometrically. It also offers the advantages of being simple, cheap, straightforward analysis, reasonable sensitivity, and reproducibility.

$$H_2BO_3^- + H^+ \xrightarrow{k_1} H_3BO_3 \quad \text{Almost instantaneous} \quad \text{reaction(i)} \quad (1)$$

$$5I^- + IO_3^- + 6H^+ \xrightarrow{k_2} 3I_2 + 3H_2O \quad \text{Very fast} \quad \text{reaction(ii)} \quad (2)$$

The acid-base neutralization reaction (reaction i) competes with the oxidation-reduction reaction, also called Dushman reaction (reaction ii), for reacting with acid proton (H^+). The Dushman reaction is very fast but significantly slower than the instantaneous acid neutralization reaction. Dushman's reaction time is on the order of the magnitude of micromixing time, while the neutralization reaction is almost instantaneous [6,14,15,21].

Reaction rates have been determined experimentally through kinetic investigations in numerous studies [35-38]. The accepted ones are given by:

$$r_1 = k_1[H^+][H_2BO_3^-] \quad (3)$$

With $k_1 = 10^{11}\ L \cdot mol^{-1} \cdot s^{-1}$

$$r_2 = k_2[H^+]^2[I^-]^2[IO_3^-] \quad (4)$$

where the rate constant of reaction (ii) is the function of the mixture ionic strength and can be written as:

$$\begin{aligned} \log k_2 &= 9.28105 - 3.664\mu^{1/2} && \text{for} \quad \mu < 0.166\ mol \cdot L^{-1} \\ \log k_2 &= 8.383 - 1.5112\mu^{1/2} + 0.23689\mu && \text{for} \quad \mu > 0.166\ mol \cdot L^{-1} \end{aligned} \quad (5)$$

The ionic strength μ is defined as:

$$\mu = \frac{1}{2} \sum_{i=allspecies} C_i z_i^2 \quad (6)$$

where C_i and z_i are the molar concentration (mol/L) and the charge number of ion i, respectively.

As mentioned, the Villermaux-Dushman method is based on competition between a very fast and an instantaneous reaction. The sulfuric acid concentration must be in stoichiometric deficit

to ensure that two reactions will compete with each other. Hence, feeding a small amount of acid to the buffer solution makes the product produced depend on the quality of mixing [31,39]. The acid is instantly dispersed locally and globally within the reactive mixture under perfect mixing conditions; thereby, it is instantaneously neutralized by borate ions (reaction (i)) due to the higher reaction rate than the redox reaction. In this case, reaction (ii) does not proceed and the amount of iodine formed is zero.

When the micromixing time is on the order of magnitude or greater than the characteristic time of the Dushman reaction, micromixing is poor. In this case (imperfect micromixing), local consumption of $H_2BO_3^-$ by reaction (i) subsequently leads to local overconcentration of acid protons, which makes the reaction (ii) occur and yields iodine. Thus, the H^+ ions are consumed competitively by the above reactions in partial segregation conditions. Therefore, the more iodine produced makes the micromixing process less ideal and vice versa. The iodine produced in reaction (ii) will react with excessive iodide ions present in the mixture to produce triiodide ions, according to the following reaction:

$$I_2 + I^- \overset{K_{eq}}{\longleftrightarrow} I_3^- \quad \text{quasi-instantaneous equilibrium} \quad \text{reaction (iii)} \tag{7}$$

$$K_{eq(iii)} = \frac{[I_3^-]}{[I_2][I^-]} \tag{8}$$

The chemical equilibrium constant is related to the reaction temperature T [K] by the following equation:

$$\log K_{eq(iii)} = \frac{555}{T} + 7.355 - 2.575 \log T \tag{9}$$

The $K_{eq(iii)}$ value at 20 °C equals 786 L/mol. The kinetics of the reaction is written as follows [15,40]:

$$r_3 = r_3^+ - r_3^- = k_3^+[I^-][I_2] - k_3^-[I_3^-] \tag{10}$$

At 25 °C:

$$k_3^+ = 5.9 \times 10^9 \ \text{Lmol}^{-1}\text{s}^{-1} \text{ and } k_3^- = 7.5 \times 10^6 \ \text{s}^{-1}$$

The amount of triiodide I_3^- at the reactor outlet can be determined by UV-VIS spectrophotometry at λ=353 nm. Therefore, the selectivity of the iodine formed can be used to quantify the fluid segregation and quantitatively express the micromixing efficiency. The segregation index, X_S, is a criterion that indicates the quality of micromixing, defined as the relative amount of fraction of acid consumed to produce the unwanted product (iodine). Therefore, lower values of X_S correspond to better micromixing. The value of this index (X_S) is in the range of 0 and 1 and is defined as [37,38]:

$$X_S = \frac{Y}{Y_{ST}} \tag{11}$$

In perfect micromixing, X_S equals 0, and in total segregation, it equals 1. Y is the ratio between the number of acid moles consumed by reaction (ii) and the total number of acid moles injected, representing the iodine (undesired product) yield given by Eq. (12).

$$Y = \frac{2(n_{I_2} + n_{I_3^-})}{n_{H_0^+}} \tag{12}$$

For continuous flow reactors, Y is expressed based on molar flow rate with the following expression [35]:

$$Y = \frac{2F_{I_2+I_3^-}}{F_{H_0^+}} \tag{13}$$

The excess amount of iodide in the solution shifts the third equilibrium reaction (Eq. (7)) to the right, and all iodine is completely reacted to form triiodide. Thus the iodine concentration is assumed to be zero:

$$Y \cong \frac{2F_{I_3^-}}{F_{H_0^+}} = \frac{2Q_{I_3^-}[I_3^-]}{Q_{H_0^+}[H^+]_0} \tag{14}$$

For total segregation corresponding to infinitely slow mixing, the maximum theoretical yield of iodine, Y_{ST}, is defined. In this case, the two reactions (i) and (ii) are instantaneous concerning the mixing rate. Therefore, the acid is consumed in proportion to the local concentrations of borate and iodide-iodate [37].

$$Y_{ST} = \frac{6[IO_3^-]_0}{6[IO_3^-]_0 + [H_2BO_3^-]_0} \tag{15}$$

In the above equations, n, F and Q represent the molar amount, molar flux and molar flow rate, and subscript 0 corresponds to the initial state at zero time. Finally, X_S is calculated as:

$$\begin{aligned} X_S &= \frac{Y}{Y_{ST}} = \frac{2Q_{I_3^-}[I_3^-]/Q_{H_0^+}[H^+]_0}{6[IO_3^-]_0/(6[IO_3^-]_0 + [H_2BO_3^-]_0)} \\ &= \frac{Q_{I_3^-}[I_3^-]}{Q_{H_0^+}[H^+]_0}\left(2 + \frac{[H_2BO_3^-]_0}{3[IO_3^-]_0}\right) \end{aligned} \tag{16}$$

The triiodide concentration is the only unknown variable that is determined by measurement of absorption intensity at 353 nm by spectrophotometry and application of Beer-Lambert's law [11,37]:

$$[I_3^-] = \frac{A}{\varepsilon_{353} l} \tag{17}$$

where A, ε_{353}, and l correspond to the light absorption, the extinction coefficient of triiodide ions at the wavelength of 353 nm, and the length of the optical path of the measuring cell, respectively [41].

The extinction coefficient of triiodide ions at λ=353 nm determined from the calibration curve equals 3,436 m^2/mol.

2. Incorporation Model Theory

The segregation index varies with the initial concentration of solutions, while micromixing models are independent of concentration and can be compared despite different initial concentration. So, the segregation index alone is insufficient to evaluate the micromixing quality and estimate the micromixing time, t_m. Concentration-independent models provide the possibility of comparing with past studies.

Several models have been developed to estimate the micromixing time based on the segregation index [5,42]. Among the different proposed models, the incorporation model has been widely applied for its simplicity in calculating the micromixing time in different reactors, including batch and continuous flow reactors. The incorporation model was derived from Villermaux's earlier studies and described completely by Fournier et al. Based on this model, solution 2, which has a smaller volume than other solutions (acid solution in our experiment), is divided into aggregates. The acid

aggregates are progressively invaded by solution 1 (Borate Buffer solution), which surrounds them. While the reactions occur in the aggregates, they gradually grow and become incorporated with the surrounding fluid. The characteristic time of the model is considered equal to the characteristic mixing time on the molecular scale named micromixing time. The micromixing time, t_m, represents the time at which mixing is assumed to be accomplished. The growth of the aggregate is assumed to be described by the following equation:

$$V_2=V_{2,0}\cdot g(t) \tag{18}$$

where

- $V_2(t)$: acid aggregate volume at t≠0
- $V_{2,0}$: initial acid aggregate volume at t=0
- g(t): incorporation growth function

The incorporation function depends on the incorporation mechanism and can be described in linear or exponential form as follows:

$$\text{Linear: } g(t)=1+\frac{t}{t_m} \tag{19}$$

$$\text{Exponential: } g(t)=\exp\left(\frac{t}{t_m}\right) \tag{20}$$

The incorporation function, g(t), is a function of micromixing time, t_m, for both models. In a linear function, the incorporation flow is constant, and for an exponential function, the flow is proportional to the instantaneous aggregate volume. The species concentration in the reactional volume 2 varies due to chemical reaction and transfer from fluid 1 to 2. The equations of the incorporation model proposed by Fournier are expressed using differential equations in Eq. (21).

$$\frac{dC_j}{dt}=(C_{j,10}-C_j)\frac{1}{g(t)}\frac{dg(t)}{dt}+r_j \tag{21}$$

where C_j stands for the species j concentration and $C_{j,10}$ denotes the species j initial concentration in solution 1 (Borate buffer surrounding solution which has been travelled to acid aggregates). In this equation, r_j is the rate of production of species j by the reaction, and the g(t) function is responsible for the rate of mass transfer between the aggregates, as discussed above [2,43].

3. Ultrasonic Atomization Process Theory

Ultrasonic spray nozzles generate uniform micron-sized droplets by feeding a liquid at a specified rate through a small orifice at the end of the nozzle tip vibrating longitudinally using ultrasonic piezoelectric transducers. Harmonic vibrations of transducers pulverize the thin film of liquid flowing on the atomizing surface of the nozzle into an aerosol. This process is referred to as ultrasonic atomization [44].

The ultrasonic spray nozzle system is equipped with a pair of resonating piezoelectric transducers located inside the nozzle body. A high-frequency electrical current causes the transducers to expand and contract. The frequency of the signal is the frequency of the nozzle. The tip vibrates in an axial motion, and the amount of vibration depends on nozzle frequency and power level applied. When liquid is fed through the center of the horn of the resonating nozzle, surface waves will form on the atomizing surface due to ultrasonic vibration [26,29,45].

The disintegration mechanism consists of breaking up liquid into liquid threads or sheets and then into droplets is a common phenomenon in almost every type of atomization process. The liquid disintegration mechanism during ultrasonic atomization has been reported in many literature studies [25,46]. Mechanical vibration of the nozzle actuates the ultrasonic horn, and liquid spreads over the atomizing surface to create surface waves. The unstable surface waves formed at the nozzle tip-free surface of the liquid film play a vital role in atomization and are responsible for droplet formation. Droplet formation results in two stages: wave creation on the liquid film surface followed by drop break-up and detachment from wave peaks. When the system reaches the resonant frequency, the oscillation amplitude is sufficient to generate these waves on the film liquid surface (regular alternation of troughs and peaks). When the wave amplitude increases, the wave peaks stretch and become taller, and the troughs of the waves become deeper until the capillary waves become unstable. This instability causes the wave peaks to become loose and detach from the bulk of the liquid film. In the next cycle of oscillation, the ridge that has just formed a drop retracts to form a hollow, while ridges form from the surrounding hollows and, in turn, create drops. The small droplets ejected from the collapsing waves generate a low-velocity fine uniform spray [26,47,48].

EXPERIMENTAL

1. Examined Concentration Set of Dushman Reaction

The Beer-Lambert law, which relates the absorbance of triiodide to its concentration, is only linear at low absorbance values. Thus, the reactant concentrations must be selected to keep the measured absorbance within the linear range [10]. The examined set of concentrations has been proposed by the works of the group of Villermaux [31], and Commenge and Falk [40] provided the basis for this experiment (Table 1). This is the most common set of concentrations used in characterizing mixing studies [8,21,38,41].

Different acid concentrations, including 0.0125, 0.025, 0.05 mol/L corresponding to 0.025, 0.05 and 0.1 H^+ concentration, respectively, were tested. The H^+ concentrations are referred to as a complete theoretical dissociation.

2. Solution Preparation

The borate buffer solution and the sulfuric acid solution were prepared based on the concentrations provided in Table 1. The buffered solution (Solution 1) was prepared as follows: Initially, NaOH and H_3BO_3 were dissolved in deionized water. Then the as-pre-

Table 1. The list of the concentrations of the reactants

Solution	Chemical	Concentration (mol/L)
Buffered solution	Potassium iodide (KI)	0.01167
	Potassium iodate (KIO_3)	0.00233
	Orthoboric acid (H_3BO_3)	0.1818
	Sodium hydroxide (NaOH)	0.0909
Acid solution	Sulfuric acid ($H_2SO_{4)}$	0.0125, 0.025, 0.05

pared solutions were mixed to produce a buffer solution at pH 9.14. Afterwards, iodide and iodate solutions were prepared by dissolving potassium iodide and potassium iodate in deionized water. Iodide/iodate solution was prepared by mixing KI and KIO_3 solutions. Subsequently, iodide/iodate solution and buffer solution were mixed and excessive deionized water was added to obtain 1 L of this solution [8,31,41,49].

The sulfuric acid solutions (Solution 2) were prepared by diluting concentrated H_2SO_4 in deionized water. The concentration of H_2SO_4 solution was 0.0125, 0.0250 and 0.05 mol/L, corresponding to 0.025, 0.05 and 0.1 mol/L H^+ concentration.

3. Experimental Setup

A schematic sketch of the experimental setup is depicted in Fig. 1. It comprises four main units: the Dushman solution supply unit, gas supply unit, micromixer, and an ultrasonic atomizer system.

The rig consists of a syringe pump and a peristaltic pump used to deliver the inlet reagent streams to the Y-micromixer at desired flow rates through inlet channels continuously. The buffer solution flow rate was 1-12 mL/min, while the acid solution was injected at 1-4 mL/min flow rates. The mixing performance of the proposed reactor was measured at four different volumetric flow rate ratios of buffer and acid solutions (which will be described completely in section 5.1) in the range of 1 to 4.

All experiments involved injecting sulfuric acid and buffer solution into the micromixer. To evaluate micromixing performance, sulfuric acid must be in stoichiometric default to start a competition between two reactions. The reaction mixture was passed through the micromixer towards the ultrasonic atomizer using two pumps in the experiments. The micromixer was fixed in a horizontal position throughout the experiment, while the ultrasonic atomizer was clamped vertically. The flow rates were successively changed, as reported in Table 2, while the same procedure was repeated each

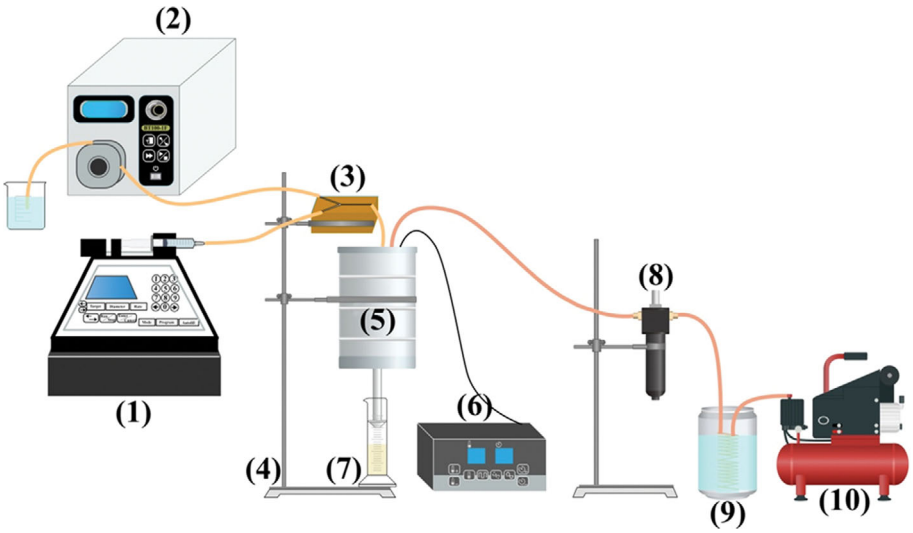

Fig. 1. Experimental setup.

(1) Syringe pump
(2) Peristaltic pump
(3) Y-micromixer
(4) Ring stand and ring clamp
(5) Ultrasonic atomizer
(6) Power generator
(7) Product container
(8) Compressed air filter
(9) Coil box cooler
(10) Oil-free air compressor

Table 2. Values of X_S in the ultrasonic nozzle atomizer reactors with and without irradiation

Test NO	Q_A	Q_B	R	$[H_2SO_4]$	Q	X_S in M-2		X_S in M-1	
						Without irradiation	With irradiation	Without irradiation	With irradiation
1	1	1	1	0.0125	2	0.046588246	0.022821394	0.00867213	0.00345581
2	2	2	1	0.0125	4	0.028450671	0.017865891	0.007237642	0.00260816
3	3	3	1	0.0125	6	0.00899815	0.00671601	0.003064587	0.00097806
4	4	4	1	0.0125	8	0.004890299	0.003781831	0.002412547	0.00071724
5	2	1	2	0.025	3	0.094871795	0.080200899	0.02831483	0.01946339
6	4	2	2	0.025	6	0.054795797	0.036237113	0.018289717	0.01515993
7	6	3	2	0.025	9	0.03405278	0.028168121	0.015624504	0.01310600
8	8	4	2	0.025	12	0.019887215	0.014964314	0.013619482	0.01166336
9	4	1	4	0.05	5	0.163009957	0.131223015	0.080200899	0.07029804
10	8	2	4	0.05	10	0.092100626	0.07759274	0.068178915	0.05921337
11	12	3	4	0.05	15	0.07628866	0.070501806	0.059539387	0.04992180

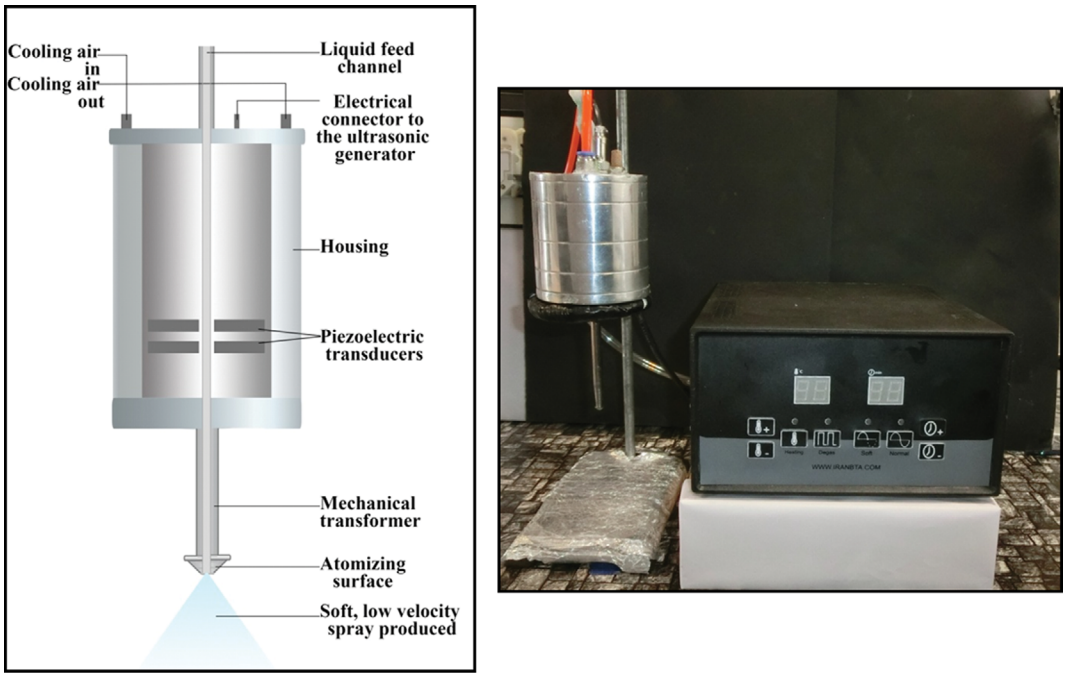

Fig. 2. Ultrasonic atomizer.

time.

Then the power generator of the ultrasonic atomizer was turned off, and the experiments were repeated in the absence of the ultrasonic irradiation. Each experiment was repeated three times, and the average values of the segregation index are reported in Table 2.

To study the influence of inlet channel size, two different micromixers, M-1 and M-2, were printed using a 3D printer. After tests of M-1 were performed, it was replaced with M-2, and the tests were undertaken (Table 2). The air supply unit issues air to the ultrasonic atomizer from an oil-free air compressor. The compressed air leaving the air compressor is not generally of a quality suitable for the intended use. The air supplied to the atomizer for cooling must be dry and clean. A small amount of dirt or moisture passing through it can cause instrument malfunction or damage to the instrument. So, air treatment is required to obtain clean, dry air to enter the atomizer. Therefore, it is essential that sufficient cooling is first carried out to fully condense any water vapor, which typically means first passing them through a sample cooler, in this case, a coil box cooler. The cooled compressed air then flows through filters. This design guarantees compressed air quality while protecting the downstream equipment of the atomizer.

In this study, simple Y-type micromixers, one of the widely used and extensively studied micromixers, were fabricated using a 3D printer. Despite the simplicity of the concept of Y micromixers, it considerably impacts the mixing efficiency. The Y-type micromixers were printed using an FDM 3D printer (Quantum Generous pro, Persia 3D Industries, Tehran, Iran).

Two Y-shaped microchannels with different internal diameters of 150 μm (M-1) and 250 μm (M-2) were designed and used. The inlet and outlet channel length was 15 mm for the two micromixers.

In FDM 3D printers, the channel can be consistently smaller than in the CAD model due to the spreading of the polymer as it is extruded. To measure the exact channel width, a red dye solution was pumped through the micromixer using a syringe pump. Different snapshots were taken with the digital microscope (dual-purpose digital microscope, model # 44325, built-in 1.3MP digital camera and equipped with 10x, 60x, 200x power (magnification)), using 200x magnification. The channel sizes and geometries were evaluated by comparing the channel width measurement using ImageJ software and a needle with a known outside diameter (21G and 20 G). The actual channel diameter of M-1 and M-2 was equal to 0.8 mm and 1.5 mm.

The Iran BTA ultrasonic atomizer constructed by Behin Tamin Ahura Company (LLC.) was used for experimentation. The ultrasonic atomizer system consists of an ultrasonic spray nozzle and power generator (Fig. 2(a)). The ultrasonic power generator supplies the electrical energy required for the operation of the ultrasonic atomizer. The power generator controls the ultrasonic frequency and power of the piezoelectric transducers. The ultrasonic nozzle is constructed from titanium alloy because of its superior acoustic properties, excellent corrosion resistance, and high strength. Housing made of stainless steel protects the internal nozzle components.

The ultrasonic atomizer composed of two piezoelectric discs tightens between a backing which acts as a mechanical amplifier and a mechanical transformer. The free end of the mechanical transformer is the conical front horn which provides the atomizing surface area. Each atomizer is designed to work at a particular resonance frequency. A schematic view of a typical ultrasonic atomizer is displayed in Fig. 2(a), and the real picture of the ultrasonic atomizer

Fig. 3. Spray generated using the ultrasonic atomizer.

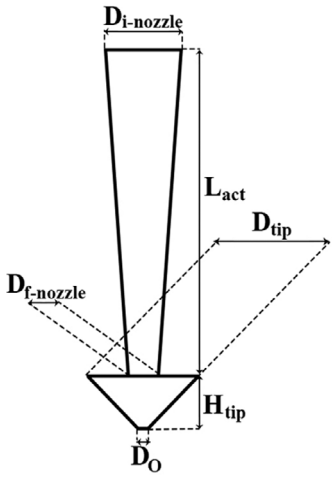

$D_{i\text{-}nozzle}$	7 mm
L_{act}	84.5 mm
$D_{f\text{-}nozzle}$	5 mm
D_{tip}	7 mm
H_{tip}	3.5 mm
D_o	0.9 mm

Fig. 4. Ultrasonic atomizer nozzle and relevant dimensions.

used in the present study is depicted in Fig. 2(b).

The liquid mixture of reactants flows downstream of the Y junction to the atomizer. The reaction mixture is supplied to the atomizer through the internal liquid feed channel (Fig. 2(a)). The liquid feed channel provided in the horn running through the length of the nozzle is a non-clogging channel with an internal diameter of 10 mm. Due to the nozzle-specific design, the reaction mixture within the nozzle only comes into contact with titanium, which is resistant to chemical attack. When the mixture is introduced into the liquid feed channel, it spreads over the atomizing surface to form a thin liquid film. The piezoelectric disk transducers receive electrical energy from the power generator and convert it into mechanical energy to actuate the ultrasonic horn at the same frequency, which is then absorbed by the liquid passing through the atomizing surface. Mechanical vibration of the nozzle transferred into the liquid induces surface waves on the liquid film surface. Then the amplitude of the waves grows, and the resonance is reached, resulting in droplet ejection from wave peaks of unstable surface waves [26,47]. Finally, the micron-sized droplets are discharged through the 0.9 mm nozzle as a mist-like uniform spray. The main factors affecting mean droplet diameter and droplet size distribution are frequency and liquid properties. Fig. 3 shows the typical image of spray ejected from the ultrasonic nozzle at the total flow rate of 10 mL/min.

The ultrasonic piezoelectric transducers worked at an operational frequency of 41.85 kHz; thus, all experiments were conducted at this working frequency. A specific resonant frequency of 41.85 kHz applied in this work dictates the mean droplet size of about 34 μm regardless of the effect of flow rate according to Lang correlation [50]. The liquid was atomized at a fixed flow rate in each experiment with a frequency of 41.85 kHz. The power of the ultrasonic power generator was set to 50 W. The power intensity was calculated by dividing the delivered power to the surface by the vibrating surface area.

The sum of three areas gives the vibrating surface area: (i) the lateral area of a truncated cone with $D_{i\text{-}nozzle}$ and $D_{f\text{-}nozzle}$ as bases and L_{act} as height, (ii) the lateral area of a truncated cone with bases D_{tip} and D_o and height H, and (iii) the annulus area with exterior and interior diameters of D_{tip} and $D_{f\text{-}nozzle}$. The relevant dimensions of the ultrasonic nozzle are illustrated in Fig. 4.

Ultrasonic energy dissipation due to the vibration and the viscous dissipation leads to an increase in liquid temperature passing through the nozzle. Liquid heating in an ultrasonic atomizer is not desirable; hence the ultrasonic spray nozzle system has air temperature control ports (Fig. 2(a)). Moreover, the transducers are temperature constrained and must be maintained at a specified temperature range. Thus, cold air was admitted into the nozzle atomizer to inhibit the rise in temperature of the piezoelectric transducers, and the liquid spreads over the atomizing surface. This was done in such a way that guaranteed the constant temperature of the reaction. Note that all experiments were conducted at room temperature.

MODEL

1. Micromixing Time (t_m) Determination

For exponential incorporation function, $g(t)=\exp(t/t_m)$, Eq. (21) transformed to the following equation:

$$\frac{dC_j}{dt}=\frac{(C_{j,10}-C_j)}{t_m}+r_j \tag{22}$$

Then the mass-balance equation (Eq. (22)) was written for each chemical species (H^+, I^-, IO_3^-, I_2, I_3^-, $H_2BO_3^-$, H_3BO_3) involved in the reactions (i-iii) by adopting the following nomenclature [5,6,13,51]:

$A=H^+$, $B=I^-$, $C=IO_3^-$, $D=I_2$, $E=I_3^-$, $F=H_2BO_3^-$, $G=H_3BO_3$

$$\frac{dC_A}{dt}=\frac{-C_A}{t_m}-r_1-6r_2 \tag{23}$$

$$\frac{dC_B}{dt}=\frac{C_{B,10}-C_B}{t_m}-5r_2-r_3^++r_3^- \tag{24}$$

$$\frac{dC_C}{dt}=\frac{C_{C,10}-C_C}{t_m}-r_2 \tag{25}$$

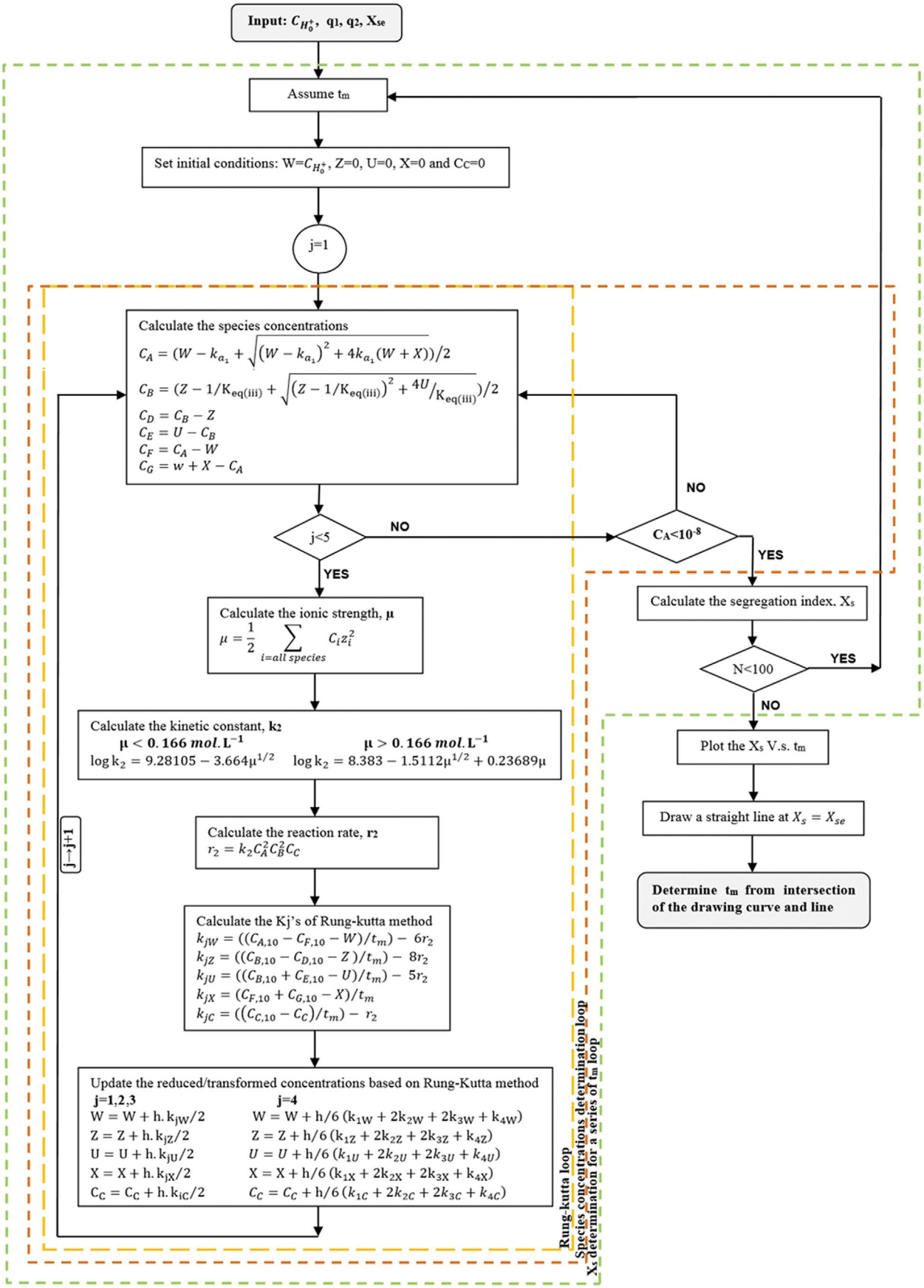

Fig. 5. Micromixing time determination of incorporation model using 4th order Runge-Kutta method (RK4).

$$\frac{dC_D}{dt}=\frac{-C_D}{t_m}+3r_2-r_3^+ +r_3^- \tag{26}$$

$$\frac{dC_E}{dt}=\frac{-C_E}{t_m}+r_3^+ -r_3^- \tag{27}$$

$$\frac{dC_F}{dt}=\frac{C_{F,\,10}-C_F}{t_m}-r_1 \tag{28}$$

$$\frac{dC_G}{dt}=\frac{C_{G,\,10}-C_G}{t_m}+r_1 \tag{29}$$

In the above equations, the difficulty lies in treating the r_1, r_3^+ and r_3^- reaction terms because reactions (i) and (iii) are instantaneous and equilibrium reactions, respectively. Thus, using the following transformations ($W=C_A-C_F$, $Z=C_B-C_D$, $U=C_B+C_E$, $X=C_F+C_G$), the r_1, r_3^+, and r_3^- reaction terms are omitted in mass-balance equations. The transformed equations are as follows:

$$\frac{dW}{dt}=\frac{C_{A,\,10}-C_{F,\,10}-W}{t_m}-6r_2 \tag{30}$$

$$\frac{dZ}{dt}=\frac{C_{B,\,10}-C_{D,\,10}-Z}{t_m}-8r_2 \tag{31}$$

$$\frac{dU}{dt}=\frac{C_{B,\,10}+C_{E,\,10}-U}{t_m}-5r_2 \tag{32}$$

$$\frac{dX}{dt}=\frac{C_{F,\,10}+C_{G,\,10}-X}{t_m} \tag{33}$$

Eqs. (30)-(33) and Eq. (25) with known initial concentrations based on experimental conditions can be solved by assuming a value for t_m. These differential equations were solved using the fourth-order Runge-Kutta (RK4) method for the initial conditions ($W=C_{H_0^+}$, $Z=0$, $U=0$, $X=0$, and $C_C=0$). Due to the earlier transformations, the species concentrations were not determined, and W, Z, U, X, and C_C were just calculated.

The iteration stops when the concentration of H^+ approaches zero. In this work, 10^{-8} mol/L was taken as the criterion for total acid consumption.

From the chemical equilibrium constant of reaction iii, $K_{eq(iii)}=\frac{[I_3^-]}{[I_2][I^-]}=\frac{C_E}{C_D C_B}$ and by substitution of C_D and C_E with C_B-Z and U-C_B, a quadratic equation on C_B is obtained as follows:

$$C_B^2+\left(\frac{1}{K_{eq(iii)}}-Z\right)\cdot C_B-\frac{U}{K_{eq(iii)}}=0 \tag{34}$$

By solving this equation, C_B is found. Hence C_B, C_C, C_D, and C_E are known so far. For calculating the remaining unknown species concentrations, C_A, C_F and C_G, the definition of the first dissociation constant of orthoboric acid is written:

$$k_{a_1}=\frac{[H^+][H_2BO_3^-]}{H_3BO_3}=\frac{C_A\cdot C_F}{C_G} \tag{35}$$

C_F and C_G can be substituted with C_A-W and W+X-C_A. Then, the C_A is found by solving the below quadratic equation:

$$C_A^2+(k_{a_1}-W)\cdot C_A-k_{a_1}(W+X)=0 \tag{36}$$

k_{a_1} is equal to 5.8×10^{-10} mol/L in water at 25 °C [52].

Finally,

$$r_2=k_2=k_2[H^+]^2[I^-]^2[IO_3^-]=k_2C_A^2C_B^2C_C$$
$$=k_2C_C\left(\frac{Z-1/K_{eq(iii)}+\sqrt{(Z-1/K_{eq(iii)})^2+4U/K_{eq(iii)}}}{2}\right)^2$$
$$\cdot\left(\frac{W-k_{a_1}+\sqrt{(W-k_{a_1})^2+4k_{a_1}(W+X)}}{2}\right)^2 \tag{37}$$

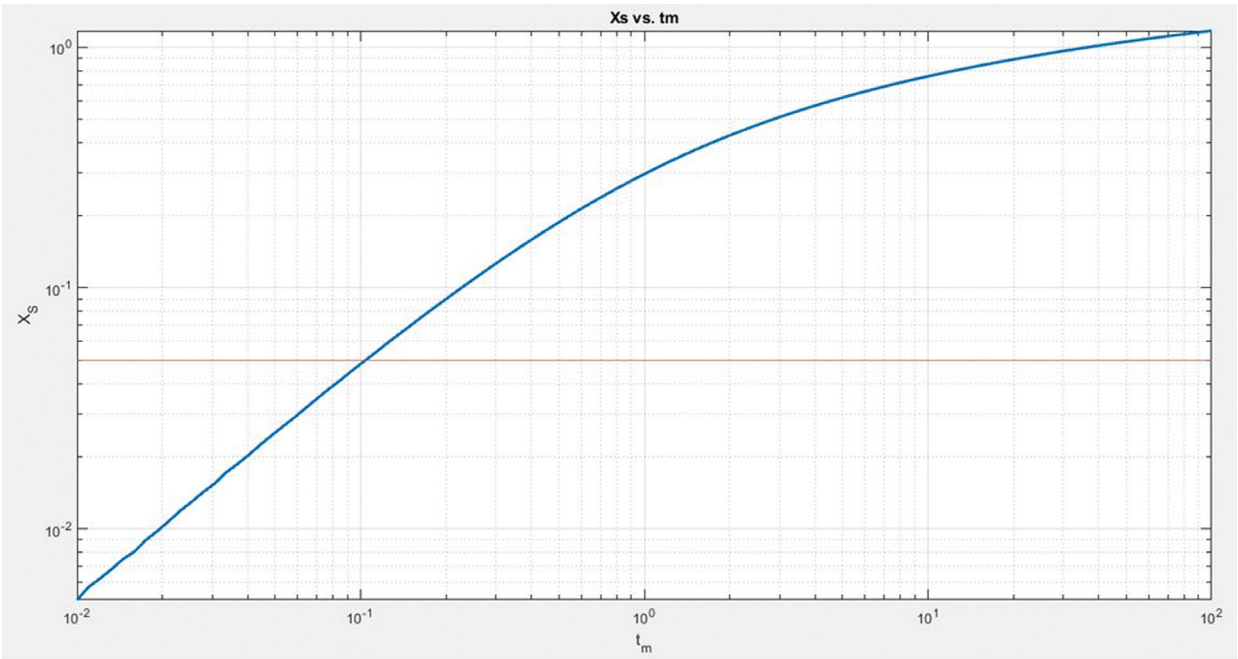

Fig. 6. Micromixing time plot for test #11 (M-1 micromixer, with irradiation).

The final calculated species concentrations of all substances allow the calculation of the segregation index correspondingly according to its definition (Eq. (16)). The theoretical value of X_S for each presumed value of micromixing time is calculated using this procedure.

The procedure for finding micromixing times consists of assuming a series of t_m, solving the reduced equations (Eqs. (25), (30)-(33)), and calculating concentrations of the species correspondingly. Species concentrations found by the Runge-Kutta iterative method, are updated during each iteration step, and the kinetic data. The theoretical X_S is calculated from the final concentration data, corresponding to the presumed t_m. The algorithm developed for these calculations is shown in Fig. 5.

Different theoretical segregation indexes are produced by applying the algorithm mentioned above for many micromixing times. Next, the calculated segregation indexes versus the t_m are plotted. A straight line is drawn at the experimental segregation index to facilitate the determination of micromixing time.

The script is run for different experimental conditions, i.e., experiments in the presence and absence of ultrasonic irradiation. Fig. 6 represents the plot of X_S vs. t_m for test 11 (Table 2) in the M-1 micromixer and in the presence of ultrasonic irradiation.

RESULTS

The effects of acid concentration at the constant acid volumetric flow rate, the acid concentration at constant base volumetric flow rate, base volumetric flow rate, total volumetric flow rate, ultrasonic, and the inlet micromixer size on the segregation index were studied. The experimental segregation indices, calculated from Eq. (16), and the variables taken in the experiments in this study are given in Table 2.

1. Effect of Initial Acid Concentration at a Constant Acid Volumetric Flow Rate

The volumetric flow rate ratio R was defined as follows to assess the influence of acid concentration and volumetric flow rate ratio on the segregation index [6,53]:

$$R = \frac{Q_A}{Q_B} \tag{38}$$

Q_A and Q_B denote the volumetric flow rates of buffer and acid solutions, respectively. To change the volumetric flow rate ratio R, Q_B may change at a constant Q_A, or Q_A may change at a constant Q_B. By increasing the flow rate ratio R (i.e., lower Q_B or higher Q_A), the acid concentration C_B increased to keep the stoichiometric ratio constant according to the following equation:

$$\frac{n_A}{n_B} = \frac{Q_A}{Q_B}\left(\frac{C_A}{C_B}\right) = R\left(\frac{C_A}{C_B}\right) \tag{39}$$

Accordingly, at constant n_A/n_B, each volumetric flow rate ratio, R, corresponds to a specific acid concentration since the buffer solu-

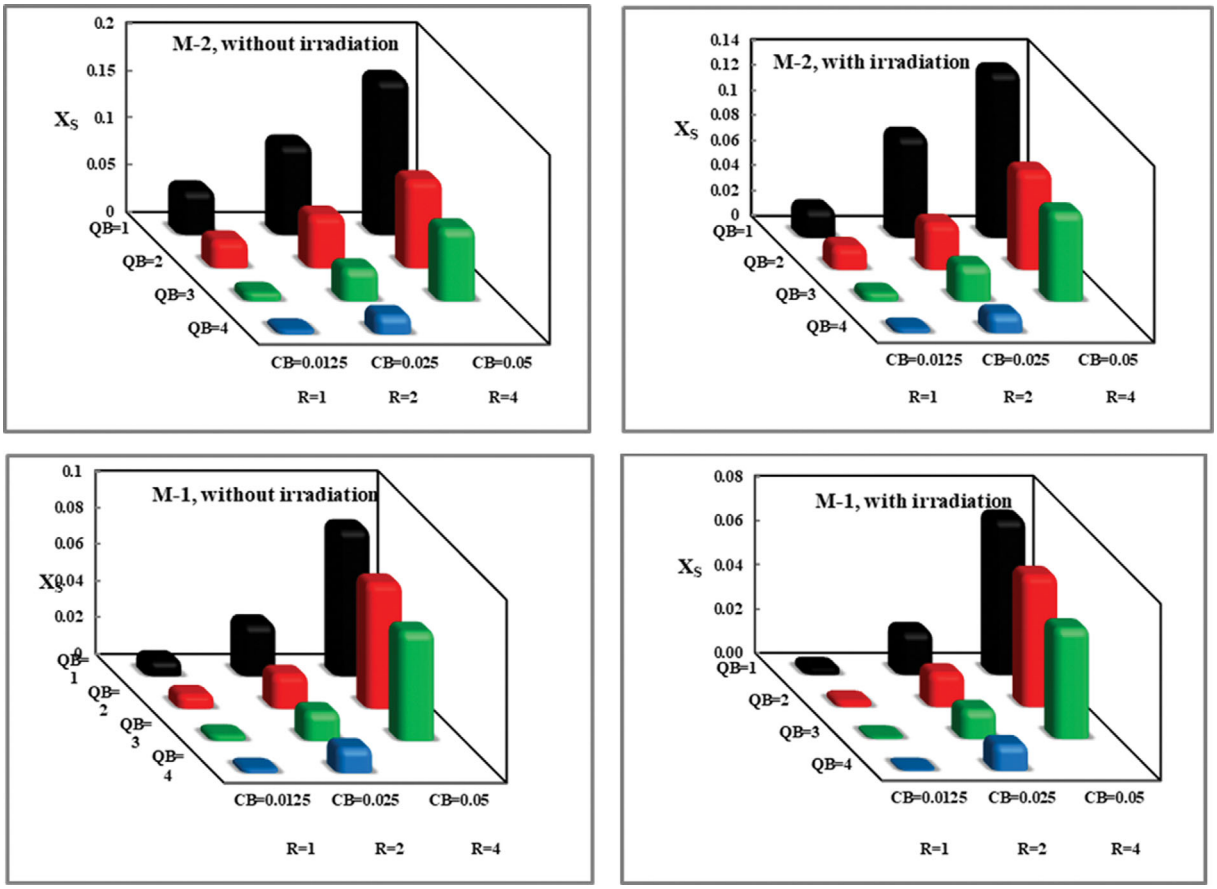

Fig. 7. Effect of initial acid concentration at constant acid volumetric flow rate and volumetric flow ratio on the segregation index.

tion is constant in all experiments, as indicated in section 3.1 (Table 1). The experiments were conducted for three different concentrations of acid, 0.0125, 0.025, and 0.05 mol/L, to assess their influence on segregation indices which correspond to R=1, 2 and 4 flow rate ratios, respectively. Two test series were carried out to investigate the effect of acid concentration and, consequently, volumetric flow rate ratio. For this purpose, the acid concentration was changed at constant Q_A and Q_B.

In the first part of the experiments, the acid flow rate Q_B was fixed, and different buffer flow rates Q_A in the range of 1-12 mL/min were applied to adjust the R-value. For example, if the initial acid concentration is halved, the base flow rate should become half too, since the n_A/n_B ratio is constant (see Eq. (39)).

Fig. 7 exhibits the influence of acid concentration on X_S measured in the atomizer setup with the different inlet micromixers in the presence and absence of ultrasonic irradiation. They represent the effect of acid concentration and flow rate ratio on the segregation index at four different acid volumetric flow rates.

As shown in the figures, the segregation indices remarkably increase in all cases by increasing the acid concentration and the corresponding R-value. It can be noticed that, for a given micromixer at constant acid volumetric flow rates, under four examined fixed acid volumetric flow rates, the segregation index increases similarly in both setups as the acid concentration increases. The reason is that the acid is consumed competitively by reactions (i) and (ii); with regards to reaction rates (Eqs. (3) and (4)), the Dushman reaction is more sensitive to acid concentration since the order of reaction with respect to acid concentration is twice of the neutralization reaction [6,8,38]. So, as the acid concentration increases, the Dushman reaction accelerates more, and more iodine is produced accordingly. Thus more triiodide will be produced, and the Y value in Eq. (12) will be larger, which leads to a larger segregation index (i.e., poor micromixing efficiency). On the other hand, a lower acid concentration notably makes the Dushman reaction slower. In this case, less iodine is produced, leading to a lower X_S, meaning an intensified mixing. Thus, it can be stated that the production of triiodide is more sensitive to acid concentration. Hence as a result of increasing acid concentration, the micromixing efficiency is reduced, and X_S is increased. Results clearly indicate that the segregation index depends on the acid concentration. The minimum value of X_S was achieved at the lowest acid concentration (0.0125). From Fig. 7, the segregation index increases as the acid concentration increases from 0.0125 to 0.05 mol/L. In fact, X_S increases sharply by increasing acid concentration. At the same time, Fig. 7 shows the effect of the volumetric flow rate ratio on the segregation index at four acid volumetric flow rates. The influence of the volumetric flow rate ratio is similar to the effect of acid concentration at a constant acid volumetric flow rate since each R-value corresponds to a specific acid concentration at a constant acid volumetric flow rate. Hence, X_S values increase by increasing the flow rate ratio.

As seen from Fig. 7, in low volumetric flow rate ratios, $X_S<0.05$ indicates excellent micromixing efficiency; however, the micromixing efficiency decreases out of this range. So, the effect of R can be explained using macromixing status as follows. Contact between streams A and B is essential for mixing the reactants to conduct the reaction. At lower R values, mixing of A and B solutions is much easier, while at larger flow rate ratios, for example, at R=4, for contacting each piece of B with four pieces of solution A simultaneously, stronger macromixing is needed, which needs a longer time and leads to a worse mixing efficiency (larger X_S) [7].

The effect of the acid volumetric flow rate Q_B at the constant acid concentration on the segregation index is also included in Fig. 7. Under constant acid concentration conditions, Fig. 7 indicates that segregation index values decrease with increasing acid volumetric flow rates. That is, the mixing performance is intensified at higher acid volumetric flow rates. This is straightforward as higher acid volumetric flow rates lead to a more intensified collision between A and B in the Y confluence junction and thus induce better mixing. The other reason is that the residence time of the acid solution in the micromixer and the ultrasonic atomizer is reduced with an increase in the acid volumetric flow rate. The decrement in acid residence time at constant acid concentration decreases the effective local overconcentration of H^+ ions. Lower local acid concentration notably makes the Dushman reaction slower, while the neutralization reaction occurs instantaneously. The less iodine production by reaction(ii) implies good micromixing efficiency (lower X_S).

By analysis, it was found that the segregation index decreases with increasing acid volumetric flow rate at constant acid concentration and decreases with decreasing acid concentration at the constant acid volumetric flow rate, indicating good micromixing efficiency. In conclusion, it was found that good micromixing efficiency (small X_S) can be obtained by increasing acid volumetric flow rate at a constant acid concentration or decreasing acid concentration at a constant acid volumetric flow rate. Therefore, low acid concentration and high acid volumetric flow rates are favorable for enhancing mixing performance. These results agree with other authors' previous results reported in the literature [6,21,49].

2. Effect of Initial Acid Concentration at a Constant Base Volumetric Flow Rate

As mentioned, the experimental investigation included two series. For the second series of experiments, different acid volumetric flow rates were fed in the ultrasonic nozzle setup at constant basic incoming fluid flow rates. During these experiments, the extent of reduction in the local concentration of the injected H^+ (reduction of the amount of injected acid) at lower acid volumetric flow rates was compensated by increasing acid concentration to maintain the stoichiometric ratio of n_A/n_B constant (see Eq. (39)). For example, if the acid flow rate is halved, the acid concentration must be doubled.

The influence of the acid concentration (or volumetric flow ratio) at a constant base volumetric flow rate (Q_A=4 mL/min) is presented in Fig. 8 for two mentioned setups with different micromixers in cases of the presence and absence of ultrasonic irradiation. The figures demonstrate that at a constant base volumetric flow rate, the segregation index (X_S) can be plotted as a function of acid concentration, volumetric flow ratio, or even acid volumetric flow rate.

The figures indicate that segregation index values increase substantially with the increase in acid concentration or volumetric flow ratio, as stated in the previous section. That is, the mixing performance is enhanced at lower concentrations of the acid solution and lower volumetric flow rate ratios. The possible reasons for this

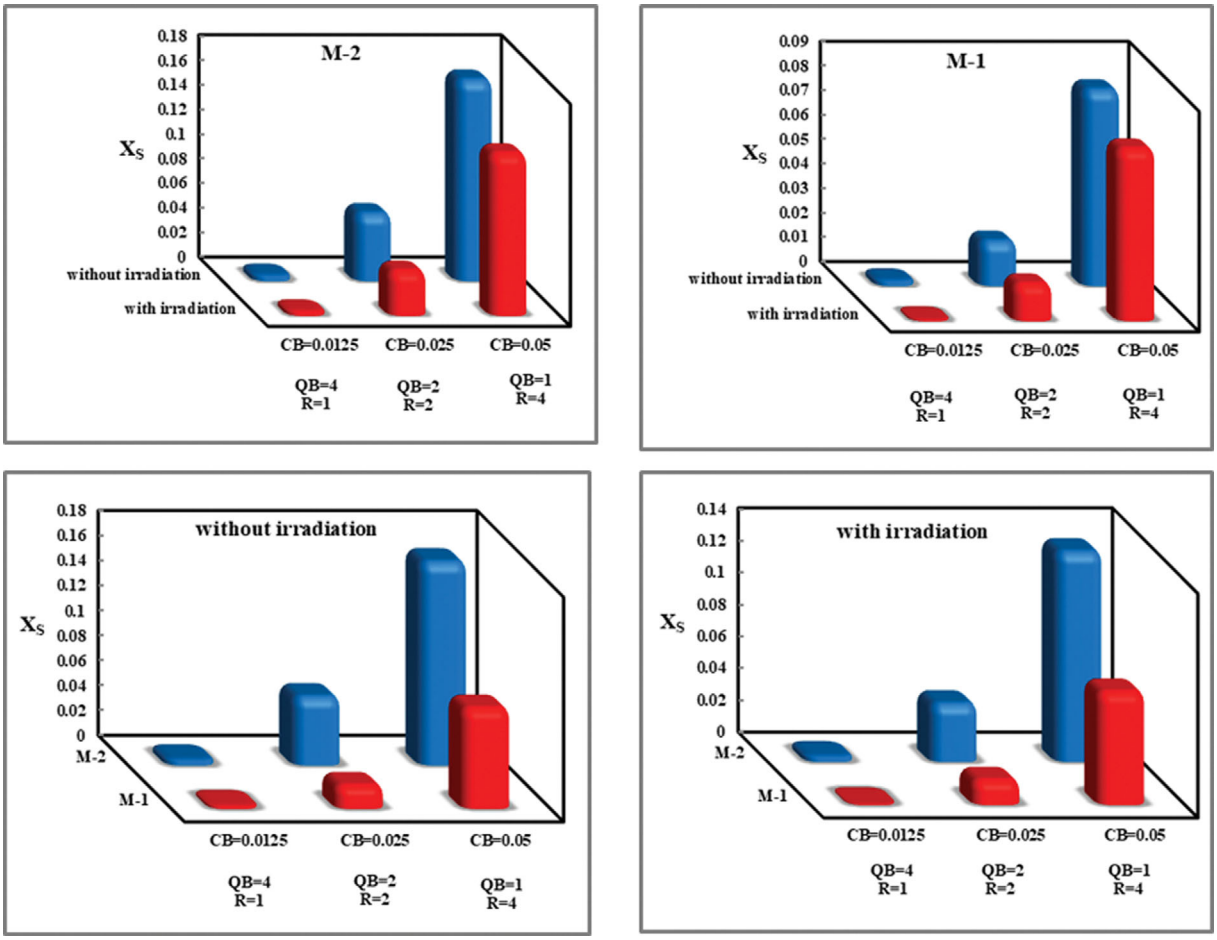

Fig. 8. Effect of initial acid concentration at constant base volumetric flow rate and volumetric flow ratio on the segregation index.

can be summarized as follows. The first reason ascribed to the higher order of rate equation of Dushman reaction with respect to acid was described in detail in section 5.1. The other reason is that, as the acid concentration C_B increases at a constant flow rate of A, Q_B will decrease to keep the stoichiometric ratio constant. The decay of Q_B at a constant flow rate of A led to a less intensive collision between A and B at the confluence; hence the segregation values were enhanced. However, depending on the flow rate, in the first stage, the mixing was controlled by the molecular diffusion and convection in the microchannels. The variation in the segregation index could also be related to molecular diffusion [54].

A similar trend is also observed for the influence of the acid volumetric flow rate. The higher the acid volumetric flow rate, the lower the values of the segregation index obtained. The reasons for this were discussed before, and this argument is described in detail in the previous section. The results of this section are consistent with the previous results.

3. Effect of Base Volumetric Flow Rate on X_S

For exploring the influence of buffer volumetric flow rate on micromixing performance, Q_A must be varied. The plots of segregation index vs. base volumetric flow rate were derived from experimental data under identical conditions (increasing C_B at constant Q_B) presented in section 5.1. Fig. 9 depicts the results for the two inlet micromixers before and after employing ultrasonic irradiation to the reaction media. Figures indicate that the X_S changes with the base volumetric flow rate. As analogous to the effect of initial acid concentration at the constant acid volumetric flow rate, the general trend of the results shows that with an increase in the flow rate, X_S values increase; hence the same discussion is applied to the reasons.

4. Effect of Total Volumetric Flow Rate on X_S

The liquid flow rate directly affected the reactor throughput in chemical reactions. In addition, the role of flow rate in mixing performance is quite obvious. So, studying the effect of liquid flow rate has significant importance. In this work, the effect of the total volumetric flow rate (acid and buffer solution flow rate) was investigated and plotted in Fig. 10. As shown in the figures, the segregation index decreases with the increase in total flow rate, which is attributed to the higher velocity of the streams. With an increase in the velocity, more intensified impinging in the convergence region will occur in the micromixer, contributing to more efficient mixing. Moreover, as the total flow rate increases, the energy dissipation rate increases with the volumetric flow rate, further enhancing the micromixing efficiency. The more enhancement in the micromixing performance makes the neutralization reaction proceed more; hence most H^+ reacts with borate ions (Eq. (1)), and the amount of iodine formed is almost zero (Smaller X_S). In conclusion, lower X_S values indicate better micromixing efficiency, so a

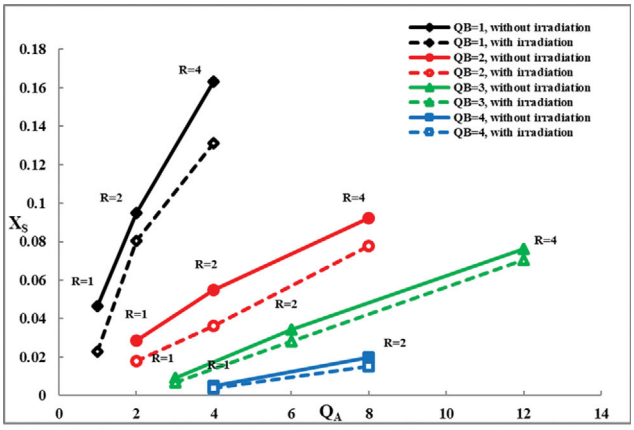

(a) M-2

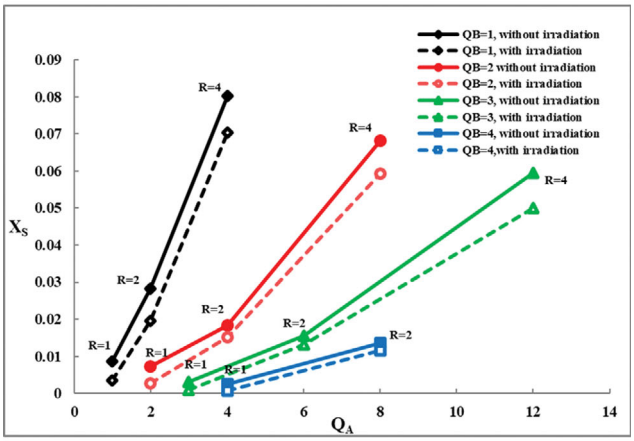

(b) M-1

Fig. 9. Effect of base volumetric flow rate on the segregation index for two micromixers.

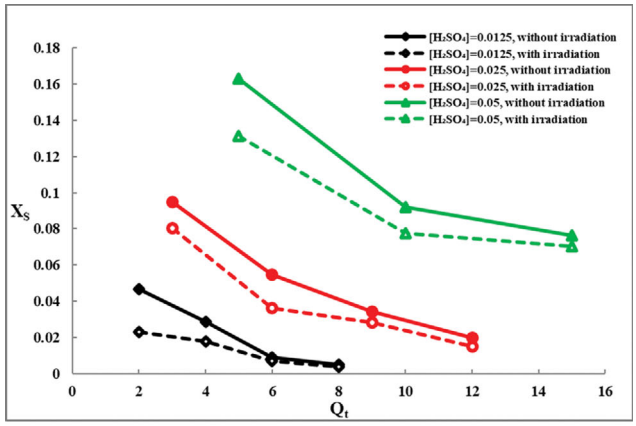

(a) M-2

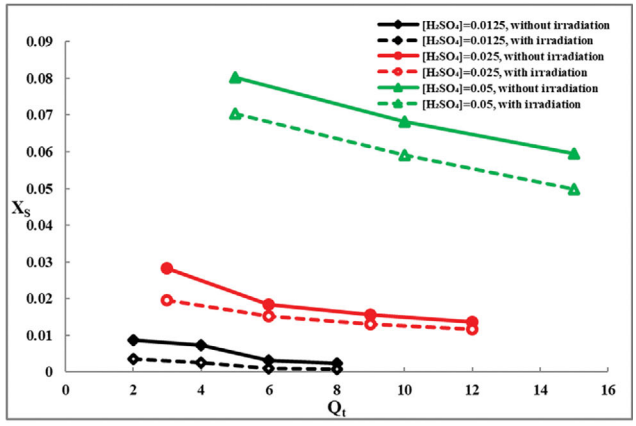

(b) M-1

Fig. 10. Effect of total volumetric flow rate on the segregation index for two micromixers.

high volumetric flow rate is favorable for the mixing of reactants.

At higher volumetric flow rates, it was found that X_S decreases more slowly with increasing flow rates. This is ascribed to the fact mentioned above, where the more enhanced micromixing efficiencies make the acid consumed by reaction (i). The trends of these figures are similar to the results previously reported by [3,6,21,34,49].

5. Effect of Inlet Micromixer Diameter on X_S

As a matter of fact, in the ultrasound spray nozzle atomizer, the mixing is accomplished both in the micromixer and the following ultrasound spray nozzle chamber. The inlet micromixer plays an important role in the mixing performance since, in the inlet micromixer, the reactant solution streams make contact first at the confluence point. Hence, to assess the influence of the inlet micromixer size on the mixing performance and find its contribution, two apparatuses with different inlet micromixers were tested. The variation of X_S in the atomizer setup with M-1 (ID of 0.8 mm) and M-2 (ID of 1.5 mm) were compared. By comparing the obtained values of X_S in the two setups, differences in mixing efficiency will be ascribed to the inlet micromixer. Hence the effect of inlet micromixer size on micromixing can be determined.

The effect of micromixer confluence shape on mixing has been investigated earlier by other authors. The mixing performance of simple designs of T, Y and arrow-shaped (oriented Y) micromixers has been compared and characterized by the Villermaux-Dushman protocol in these studies [6,14]. Among these simple design micromixers, the arrow-shaped micromixer offered the best mixing performance, while the Y-shaped micromixer provided the least performance. In the present work, the least effective confluence shape (Y-type) micromixer was selected to clarify the effect of ultrasonic atomization on a chemical reaction.

Fig. 11 shows a comparison of X_S values as a function of the base flow rate for two Y-micromixers with different diameters, M-1 and M-2, at four acid flow rates in cases of the presence and absence of ultrasonic irradiation. The similar base and acid flow rate effects are observed as described comprehensively in the previous section. At the same time, the figures illustrate the influence of inlet micromixer diameter on the segregation index for two different sizes of micromixers located at the entrance of the atomizer. It can also be noticed that whichever the micromixer, the segregation index decreases when the inlet micromixer diameter decreases. In Fig. 12, the X_S change against the total flow rate for identical conditions as Fig. 11 is presented, and the same result is drawn.

The difference between X_S for the micromixers shown in the figures is quite obvious, confirming that the inlet micromixer significantly affects the mixing performance in our setup. By comparing the results, it is obvious that M-1 always provides smaller segregation indices than M-2 for equal base flow rates (Fig. 11) or

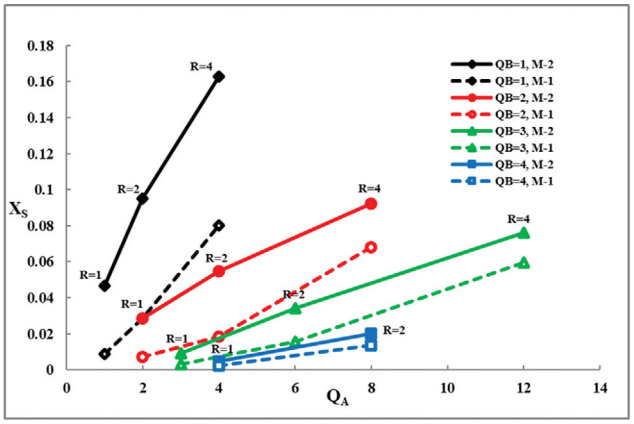

(a) Without irradiation

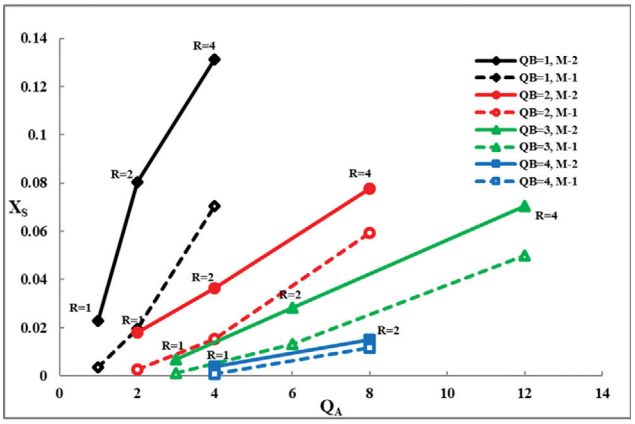

(b) With irradiation

Fig. 11. Evolution of the segregation index with the base flow rate, determining the effect of inlet micromixer diameter.

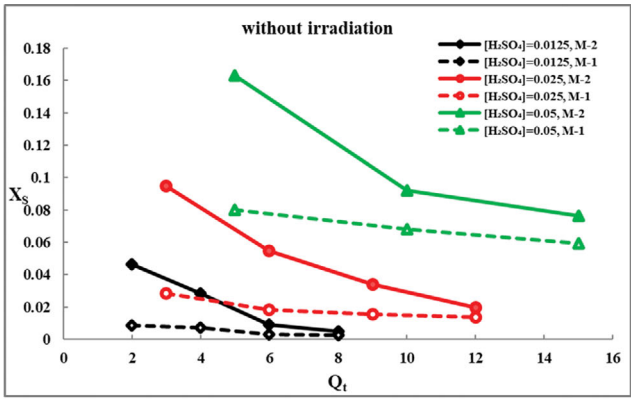

(a) Without irradiation

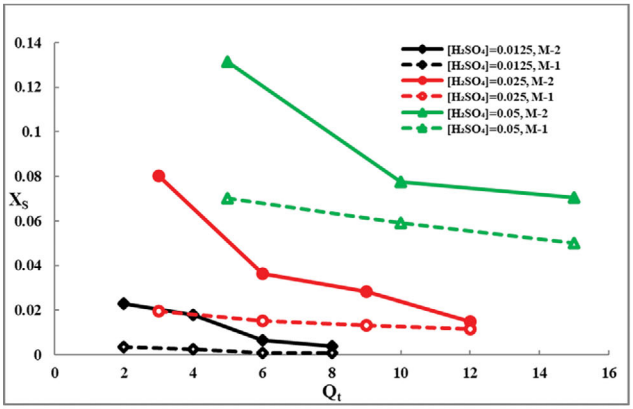

(b) With irradiation

Fig. 12. Evolution of the segregation index with the total flow rate, determining the effect of inlet micromixer diameter.

total flow rates (Fig. 12). By decreasing the size of the inlet micromixer at a constant flow rate, the following two phenomena, attributed to the two mixing mechanisms (molecular diffusion and convection), improve the mixing quality. One reason is that by decreasing the size of the inlet micromixer, fluid velocity and hence the fluid kinetic energy increases. As expected, large eddies induced by higher fluid velocity lead to enhanced interaction between the streams and an increase in energy dissipation rate. Higher energy dissipation is desirable for mixing reagents and leads to higher micromixing efficiency. The other reason is the short diffusion length between the fluid. Both relate to the small characteristic dimensions of micromixers and extremely fine droplets generated by the ultrasonic atomizer, leading to intensified mixing [3].

Thus the smaller the inlet micromixer diameter, the lower the segregation index, and therefore the better the micromixing. Furthermore, it is clear from the figures that, for a given total flow rate, the difference between micromixers segregation values is more distinct at a higher acid concentration (see Fig. 12) due to more driving forces.

Moreover, the segregation index data confirm that the effect of inlet mixer size is more significant at lower total flow rates. In comparison, at higher total flow rates, only a small effect of inlet mixer size on X_S was observed. This observation can be explained as follows. As previously discussed, X_S decreases with the increase of the liquid flow rate; however, the X_S decreases more steeply using M-2 compared with M-1, i.e., the segregation index is more sensitive in M-2.

6. Effect of Ultrasonic Wave Irradiation on X_S

Experiments were conducted with and without ultrasonic waves to explore the effect of ultrasound irradiation under the same conditions. Figs. 9 and 10 display the segregation index as the function of the base volumetric flow rate and total volumetric flow rate, respectively, in the presence and absence of ultrasonic irradiation, that is, on and off ultrasonic atomizer. It can be noticed that when the ultrasound (41.85 kHz) is present, a more efficient micromixing, i.e., lower segregation index values, is obtained compared to when ultrasound is absent. Referring to these figures, at each acid concentration, the X_S values in the presence of ultrasonic irradiation are lower than the X_S values in the absence of ultrasonic irradiation. The differences in segregation indices explain using two mechanisms of ultrasonic atomization: cavitation and capillary wave hypotheses [27,44,55].

The cavitation hypothesis is generally attributed to systems operating at high frequency and energy intensity [48]. Acoustic cavitation is obtained following the propagation of sound waves, also called pressure waves, in a liquid at rest. The implosion or collapse of the bubble causes a very high-intensity shock wave that pierces the free surface of the film and initiates its disintegration by direct expulsing of droplets [56]. This hypothesis assumes that microjets

produced by cavitation break up the capillary wave to produce atomization.

In an ultrasonic nozzle system, cavitation bubbles are formed inside the liquid film, provided that the liquid film thickness on the vibrating surface is small. During the implosion of cavitation in the liquid film, particularly cavities close to the liquid surface, high-intensity shock waves are generated. The enhanced micromixing caused by ultrasonic atomization is relevant to these hydraulic shock waves induced by cavitation [27,48].

The capillary wave hypothesis manifests by the development of capillary waves when the system resonant frequency is reached, and the oscillation amplitude is sufficient to generate these waves on the film surface (regular alternation of troughs and peaks) until they become unstable. The capillary waves become unstable and atomization occurs by tearing away the waves' peaks from the liquid bulk.

By referring to previous investigations, at low ultrasonic intensities, it was found that the droplets were produced due to the growth of capillary surface waves, while at high ultrasonic intensities, cavitation in the vicinity of the surface accompanies the development of the capillary waves to produce the fog [25,27,44,45].

The conjunction theory couples these two theories into a single theory. In the conjunction theory, the ultrasonic oscillation generates small cavitation bubbles which, by their implosion, excite the peaks of the capillary surface waves, thus causing the atomization of the liquid film. In this theory, atomization is supposed to arise from cavitation bubble implosion and capillary surface wave instability. The conjunction theory seems to be the most reasonable mechanism of droplet formation in ultrasonic atomization [27,57].

We cannot draw any conclusions about the enhanced micromixing results. However, the two mechanisms proposed to explain ultrasonic atomization, the acoustic cavitation and capillary waves, lead to an efficient micromixing of the reactants. As the result of the ultrasonic atomization, a medium is created, offering excellent conditions for intensifying micromixing and mass transfer efficiency. The results indicate that the segregation index and, consequently, the degree of the micromixing can be significantly influenced by ultrasonic atomization of the reactants.

From the above two section results, a significant conclusion can be drawn as follows: when the ultrasonic atomizer is applied in combination with a micromixer at the inlet, the effect of decrement in the inlet micromixer diameter seems to dominate the mixing in the presence of the ultrasonic irradiation in the ultrasonic atomizer. The effect of ultrasonic irradiation on micromixing seems negligible when an inlet micromixer with a certain diameter is used at the inlet.

7. Interpretation of Micromixing Time Results

Mixing time is an important parameter of fast reactions, measuring how fast the mixing process is used to assess the mixing efficiency. The principle in fast chemical reactions is based on the competition between the two characteristic time scales, i.e., micromixing time (t_m) and reaction time (t_R) [2,5,6,31,58]. The segregation index is a result of the coupling of chemical reaction processes and a mixing process which depend on the kinetics of chemical reactions (i) and (ii) (with characteristic reaction times of t_{R1} and t_{R2}) and the hydrodynamical operating conditions, respectively. Thus, the segregation index considers the influence of hydrodynamical conditions on the chemical selectivity of products [31,59].

The characteristic reaction time (t_R) of fast chemical reactions is very small. Excellent mixing in these systems is required to decrease the characteristic micromixing time, t_m, to less than the characteristic reaction time t_R for achieving a high yield and selectivity. In this case ($t_m<t_R$), the process is controlled by the intrinsic kinetics of chemical reactions and not by the micromixing; in the case of the Dushman reaction, the H^+ participates only in the quasi-instantaneous reaction (reaction i), and the second reaction does not have the chance to occur ($t_{R1}<<t_{R2}$ and $t_{R1}<<t_m$) [8,49,58].

However, when the characteristic mixing time is comparable to the characteristic reaction time, the chemical reaction is controlled by micromixing. In the case of the Dushman reaction, the H^+ ions consumed competitively by both reactions (reaction i and ii) and the micromixing efficiency can significantly affect the segregation index. The reactor should be designed in such a way as to intensify the micromixing to reach the region where $t_m<t_R$ [5,49,58].

Table 3. Comparison between mixing and residence time data

Q_A	Q_B	R	$[H_2SO_4]$	Q(I3)	M-2, without irradiation		M-2, with irradiation		M-1, without irradiation		M-1, with irradiation	
					Mixing time (s)	Residence time (s)	Mixing time (s)	Residence time (s)	Mixing time (s)	Residence time (s)	Mixing time (s)	Residence time (s)
1	1	1	0.0125	2	12.01870366	448.7372	5.601548601	448.7372	2.0681932	447.9785	0.82605102	447.9785
2	2	1	0.0125	4	7.06543156	224.3686	4.34108743	224.3686	1.72118974	223.9893	0.61276453	223.9893
3	3	1	0.0125	6	2.14753115	149.5791	1.59540127	149.5791	0.72303704	149.3262	0.23496141	149.3262
4	4	1	0.0125	8	1.15763898	112.1843	0.89317869	112.1843	0.56825438	111.9946	0.16861722	111.9946
2	1	2	0.025	3	1.84091462	299.1582	1.51233616	299.1582	0.48492498	298.6524	0.32804995	298.6524
4	2	2	0.025	6	0.98485642	149.5791	0.62941382	149.5791	0.30764534	149.3262	0.25363605	149.3262
6	3	2	0.025	9	0.58923964	99.71939	0.48230161	99.71939	0.26166443	99.55079	0.21866715	99.55079
8	4	2	0.025	12	0.33544586	74.78954	0.25025548	74.78954	0.22729191	74.66309	0.1941149	74.66309
4	1	4	0.05	5	0.41478747	179.4949	0.31419057	179.4949	0.17505276	179.1914	0.15106403	179.1914
8	2	4	0.05	10	0.20554777	89.74745	0.16857044	89.74745	0.14599425	89.59571	0.12453392	89.59571
12	3	4	0.05	15	0.16534076	59.83163	0.15154465	59.83163	0.12530358	59.73047	0.10348326	59.73047

In perfect mixing conditions or at low concentrations of reactants, hydrodynamical conditions (t_m) would have a negligible influence on X_S, and the segregation indices are very small. Therefore, to increase the sensitivity of this method, the concentration of reactants should be increased in a domain where t_{R2} is almost equal to t_m ($t_{R2} \cong t_m$) [2,31]. At the constant initial concentration of reactants and constant flow rates, the variation of X_S accurately considers the variation in t_m. In contrast, at constant hydrodynamical operating conditions, namely constant t_m, X_S only depends on chemical reaction conditions. Under non-constant reaction time and hydrodynamical conditions, micromixing analysis is more complex, and a micromixing model coupling mixing and reaction should be utilized [59].

The reaction time can be calculated directly from experimental conditions. However, the micromixing time depends on the hydrodynamic conditions, can only be determined according to experimental data by micromixing models [6,8,21,49].

Among many models, the simple and practical incorporation model was chosen for estimating the micromixing time in our continuous plug-flow reactor. At constant hydrodynamic conditions, the model is not dependent on the reactant concentrations. The incorporation model was used to extract the micromixing times from the experimental values of segregation indices. According to the described procedure in section 4 (the algorithm presented in Fig. 5), the micromixing time values were calculated for each experimental value of the segregation index for all the studied experiments presented in Table 2. Note that the model estimates the order of magnitude of micromixing time.

As discussed, $t_{R2} \cong t_m$ yields the highest sensitivity of the Villermaux-Dushman. Therefore, the reaction time must almost equal the micromixing time (small t_R) to have a high sensitivity. At the same time, too fast reaction times are not desired [2,15]. The reaction must be sufficiently slow to characterize the mixing performance throughout the reactor rather than just the initial mixing at the inlet [1]. So, the reaction time is determined due to the trade-off between characterizing the mixing performance and reaching the best possible sensitivity.

The mean residence time was calculated by dividing the reactor volume by the total volumetric flow rate.

The calculation results of micromixing time (t_m) and the residence times (τ) for all experiments listed in Table 2 are found in Table 3. From Table 3, it is clear that micromixing times are orders of magnitude smaller than residence times in all experiments, demonstrating that the reactions have been completed before UV measurements. The results in Table 3 show that at a constant volumetric flow rate ratio, the micromixing time decreases with increasing the total flow rate, confirming that the micromixing level remarkably depends on the velocity.

Fig. 13 depicts the plot of segregation indices against the calculated micromixing times for different volumetric flow rate ratios. The X_S-t_m plot (Fig. 13) gathers t_m data of two micromixers before and after applying ultrasonic irradiation on a unique curve. A linear relationship between X_S and t_m was observed in each case. The equations obtained through regression are displayed in the figure. As discussed above, the micromixing efficiency remarkably depends on the segregation index when the characteristic micromixing time

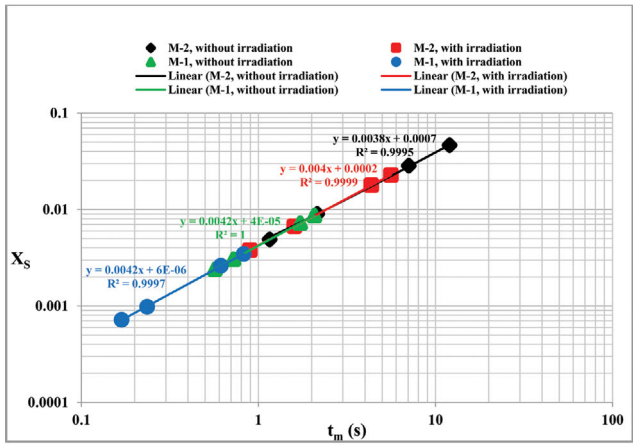

(a) R=1, $[H^+]_0$=0.025 mol/L

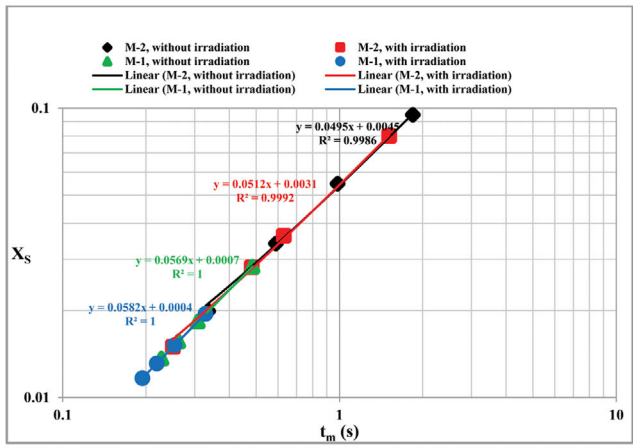

(b) R=2, $[H^+]_0$=0.05 mol/L

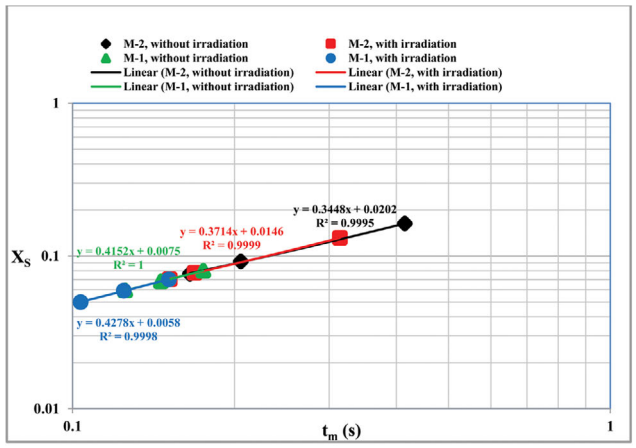

(c) R=4, $[H^+]_0$=0.1 mol/L

Fig. 13. Relationship between X_S and t_m.

is comparable to the characteristic reaction time. However, micromixing time has a negligible influence on the segregation index at low acid concentration. The regression line slope demonstrates X_S dependence on t_m, whose value is about 0.004, 0.05, and 0.4 for the acid concentration of 0.025, 0.05, and 0.1, respectively.

From Fig. 13, the X_S values are generally increased by increasing the micromixing time. The micromixing time ranging from 0.1 to 12 s was obtained according to the size of the micromixer and the

chemical reaction conditions. According to Fig. 13, micromixing times in the magnitude of 0.17-12 s, 0.19-1.84 s, and 0.1-0.4 s were observed in the volumetric flow ratios of 1, 2, and 4, respectively.

At constant volumetric flow rate ratios (Fig. 13), the highest micromixing times are obtained at the lowest volumetric flow rates among all studied flow rates, indicating poor mixing performance. The estimated micromixing times provide the possibility of comparing the micromixing levels generated by two studied micromixers and the effect of ultrasonic atomization under different experimental conditions. As illustrated, for example, for R=1, the micromixing time of M-2 and M-1 lies in the range of 1-10 s and 0.5-2 s in the absence of ultrasonic irradiation, which can reach 0.8-5 s and 0.1-0.8 s, respectively, in the presence of ultrasonic irradiation. This confirms the positive effect of the ultrasonic atomization on micromixing conditions as well as the superior micromixing efficiency of M-1 compared with M-2. M-1 generates a better micromixing level than M-2 due to its smaller hydrodynamic diameter. Furthermore, the ultrasonic atomization concept makes it possible to decrease the micromixing times. Hence, it was found to be efficient in micromixing enhancement.

The estimated micromixing times were in the range of 0.1-1 s for most operating conditions in both setups. However, the lowest micromixing times are attributed to the M-1 after applying ultrasonic irradiation, where the micromixing times exactly lie in the range of 0.1-1 s.

Note that the micromixing times in this work are higher than most of the works done in the micromixers, which are in order of milliseconds. However, Kashid et al. [42] reported that the micromixing time ranges from 0.01-10 s at 1-18 mL/min flow rates. The range of the estimated micromixing times in this work (0.1-10) is in accordance with the volumetric flow rates studied here (2-15 mL/min). Results reveal that the present novel ultrasonic atomizer reactor could simultaneously provide an enhanced medium for mixing with reaction.

From Fig. 13, a linear trendline was noticed, marked by the line crossing the data. It is clear that some points overlap each other. This indicates that the same micromixing times could be obtained in micromixers with different sizes or even before or after applying ultrasonic atomization. Therefore it can be concluded that the same micromixing performance could be provided by applying different micromixers in the presence of ultrasonic atomization or only by crossing the reaction mixture through a micromixer and a duct. This is an interesting result since the micromixing performance would result in a trade-off between different operating chemical reaction conditions and the energy dissipation costs.

CONCLUSION

This paper focused on atomizing the mixture of reactants to maximize the surface area of impingement of two reactants and increase the number of collisions between them to intensify the micromixing using an ultrasonic nozzle. The Villermaux-Dushman test reaction coupled with the incorporation model was used to study the mixing characteristics in the simple Y micromixer, followed by the ultrasonic spray nozzle atomizer as the reaction chamber.

The effects of ultrasonic irradiation and inlet micromixer diameter were considered in terms of segregation index and micromixing time by conducting the experiments in two micromixers with different diameters within the ultrasonic atomizer in the presence of ultrasonic irradiation and in the case of off ultrasonic atomizer in the absence of ultrasonic irradiation. All the experiments were conducted under various operating conditions, i.e., volumetric flow rate ratio, reactant flow rate, total flow rate, and reactant concentration.

The results confirm the positive effect of ultrasonic atomization on micromixing and the superior micromixing efficiency of smaller micromixers. The coupled system of M-1 micromixer and the ultrasonic atomizer irradiated by ultrasonic irradiation was the best combination, with segregation indices of 0.05-0.003, leading to intensified micromixing.

Based on the incorporation model, the estimated micromixing time of the reactor was found on the order of 10^{-1}-10^{0} s for the studied total volumetric flow rates, between 2 and 15 mL/min.

NOMENCLATURE

A : light absorption
C_A : molar concentration of the buffer solution [mol·L^{-1}]
C_B : molar concentration of the acid solution [mol·L^{-1}]
C_j : species j molar concentration [mol·L^{-1}]
$C_{j,10}$: species j initial concentration in buffer solution [mol·L^{-1}]
D : diameter [mm]
F : molar flux [mol·s^{-1}]
F_j : molar flux of species j [mol·s^{-1}]
g(t) : incorporation growth function
k_1 : rate constant of reaction (i) [L·mol^{-1}·s^{-1}]
k_2 : rate constant of reaction (ii) [L^4·mol^{-4}·s^{-1}]
k_3^+ : rate constant of forward reaction (iii) [L·mol^{-1}·s^{-1}]
k_3^- : rate constant of backward reaction (iii) [s^{-1}]
k_{a_1} : first dissociation constant of orthoboric acid [mol·L^{-1}]
K_{eq} : equilibrium constant of reaction (iii) [L·mol^{-1}]
l : spectrophotometer cell path length [cm]
N : mole number [mol]
n_A : moles number of the buffer solution [mol]
n_B : moles number of the acid solution [mol]
n_j : moles number of species j [mol]
Q : volumetric flow rate [mL·min^{-1}]
Q_A : buffer volumetric flow rate [mL·min^{-1}]
Q_B : acid volumetric flow rate [mL·min^{-1}]
Q_j : flow rate of species j [mL·min^{-1}]
R : volumetric flow rate ratio
r_1 : rate of reaction (i) [mol·L^{-1}·s^{-1}]
r_2 : rate of reaction (ii) [mol·L^{-1}·s^{-1}]
r_3^+ : rate of forward reaction (iii) [mol·L^{-1}·s^{-1}]
r_3^- : rate of backward reaction (iii) [mol·L^{-1}·s^{-1}]
r_j : rate of production of species j by the reaction [mol·L^{-1}·s^{-1}]
T : Temperature [K]
t_m : characteristic micromixing time [s]
t_R : characteristic reaction time [s]
t_{R1} : characteristic reaction time of reaction (i) [s]
t_{R2} : characteristic reaction time of reaction (ii) [s]
V_2 : acid aggregate volume at t≠0 [m^3]

$V_{2,0}$: initial acid aggregate volume at t=0 [m^3]
X_S : segregation index
Y : yield of iodine (undesired product)
Y_{ST} : yield of iodine at total segregation
z_i : ion i charge number

Greek Symbols

ε_{353} : molar extinction coefficient [$m^2 \cdot mol^{-1}$]
λ : absorption wavelength [nm]
μ : ionic strength [$mol \cdot L^{-1}$]
τ : residence time [s]

REFERENCES

1. C. Habchi, D. Della Valle, T. Lemenand, Z. Anxionnaz, P. Tochon, M. Cabassud, C. Gourdon and H. Peerhossaini, *Chem. Eng. Sci.*, **66**, 3540 (2011).
2. E. Tunestål, *Investigations of micromixing-In Alfa Laval's ART plate reactors*, PhD Thesis, Chalmers University of Technology, Gothenburg, Sweden (2012).
3. L. Zhendong, L. Yangcheng, W. Jiawei and L. Guangsheng, *Chem. Eng. J.*, **181**, 597 (2012).
4. G. S. Jeong, S. Chung, C.-B. Kim and S.-H. Lee, *Analyst*, **135**, 460 (2010).
5. Y. Su, G. Chen and Q. Yuan, *Chem. Eng. Sci.*, **66**, 2912 (2011).
6. M. Rahimi, N. Azimi, M. A. Parsamogadam, A. Rahimi and M. M. Masahy, *Microsyst. Technol.*, **23**, 3117 (2017).
7. W. Jiao, Y. Liu and G. Qi, *Chem. Eng. J.*, **157**, 168 (2010).
8. G.-W. Chu, Y.-H. Song, H.-J. Yang, J.-M. Chen, H. Chen and J.-F. Chen, *Chem. Eng. J.*, **128**, 191 (2007).
9. Y. Wang, X. Tao, J. Li, S. Zhang, Y. Jin and M. Chen, *Korean J. Chem. Eng.*, **38**, 1727 (2021).
10. J. M. Reckamp, A. Bindels, S. Duffield, Y. C. Liu, E. Bradford, E. Ricci, F. Susanne and A. Rutter, *Org. Process Res. Dev.*, **21**, 816 (2017).
11. M.-C. Fournier, L. Falk and J. Villermaux, *Chem. Eng. Sci.*, **51**, 5053 (1996).
12. J. Zhang, K. Wang, Y. Lu and G. Luo, *Chem. Eng. Process.: Process Intensif.*, **49**, 740 (2010).
13. K.-P. Cheng, B. Wu, R.-J. Gu and L.-X. Wen, *Micromachines*, **9**, 549 (2018).
14. O. S. Okwundu, M. Fuseini, A. H. El-Shazly and M. F. Elkady, *J. Serbian Chem. Soc.*, **85**, 381 (2020).
15. J.-M. Commenge and L. Falk, *Chem. Eng. Process.: Process Intensif.*, **50**, 979 (2011).
16. E. A. Mansur, Y. Mingxing, W. Yundong and D. Youyuan, *Chin. J. Chem. Eng.*, **16**, 503 (2008).
17. V. Hessel, H. Löwe and F. Schönfeld, *Chem. Eng. Sci.*, **60**, 2479 (2005).
18. A. Kanaris and A. Mouza, *Chem. Eng. Sci.*, **66**, 5366 (2011).
19. J. Choe, Y. Kwon, Y. Kim, H.-S. Song and K. H. Song, *Korean J. Chem. Eng.*, **20**, 268 (2003).
20. R. Singh, H.-J. Lee, A. K. Singh and D.-P. Kim, *Korean J. Chem. Eng.*, **33**, 2253 (2016).
21. M. Rahimi, P. Valeh-e-Sheyda, M. A. Parsamoghadam, N. Azimi and H. Adibi, *Chem. Eng. Process.: Process Intensif.*, **85**, 178 (2014).
22. D. Y. Kim and J. M. Kim, *Korean J. Chem. Eng.*, **36**, 837 (2019).
23. S. Bose, S. S. Keller, T. S. Alstrøm, A. Boisen and K. Almdal, *Langmuir*, **29**, 6911 (2013).
24. S. Nii, Ultrasonic Atomization, *Handbook of ultrasonics and sonochemistry*, Springer, Singapore (2016).
25. R. Rajan and A. B. Pandit, *Ultrasonics*, **39**, 235 (2001).
26. M. Dobre and L. Bolle, *Exp. Therm. Fluid Sci.*, **26**, 205 (2002).
27. B. Avvaru, M. N. Patil, P. R. Gogate and A. B. Pandit, *Ultrasonics*, **44**, 146 (2006).
28. K. C. Pingali, D. A. Rockstraw and S. Deng, *Aerosol Sci. Technol.*, **39**, 1010 (2005).
29. M. Bastwros and G.-Y. Kim, *Powder Technol.*, **288**, 279 (2016).
30. J. P. Feng, S. I. Choi, H. S. Seo and Y. M. Jo, *Korean J. Chem. Eng.*, **35**, 2001 (2018).
31. P. Guichardon and L. Falk, *Chem. Eng. Sci.*, **55**, 4233 (2000).
32. M. Assirelli, W. Bujalski, A. Eaglesham and A. Nienow, *Chem. Eng. Sci.*, **60**, 2333 (2005).
33. A. Kölbl, M. Kraut and K. Schubert, *AIChE J.*, **54**, 639 (2008).
34. S. Panić, S. Loebbecke, T. Tuercke, J. Antes and D. Bošković, *Chem. Eng. J.*, **101**, 409 (2004).
35. F. Parvizian, M. Rahimi, N. Azimi and A. A. Alsairafi, *Chem. Eng. Technol.*, **37**, 113 (2014).
36. J. Pinot, J.-M. Commenge, J.-F. Portha and L. Falk, *Chem. Eng. Sci.*, **118**, 94 (2014).
37. N. Baccar, R. Kieffer and C. Charcosset, *Chem. Eng. J.*, **148**, 517 (2009).
38. M. Faryadi, M. Rahimi, S. Safari and N. Moradi, *Chem. Eng. Process.: Process Intensif.*, **77**, 13 (2014).
39. C. Baqueiro, N. Ibaseta, P. Guichardon and L. Falk, *Chem. Eng. Res. Des.*, **136**, 25 (2018).
40. L. Falk and J.-M. Commenge, *Chem. Eng. Sci.*, **65**, 405 (2010).
41. J. Legrand, N. Benmalek, F. Imerzoukene, A.-R. Yeddou and F. Halet, *Chem. Eng. J.*, **142**, 78 (2008).
42. M. Kashid, A. Renken and L. Kiwi-Minsker, *Chem. Eng. J.*, **167**, 436 (2011).
43. M.-C. Fournier, L. Falk and J. Villermaux, *Chem. Eng. Sci.*, **51**, 5187 (1996).
44. A. Dalmoro, A. A. Barba, G. Lamberti and M. d'Amore, *Eur. J. Pharm. Biopharm.*, **80**, 471 (2012).
45. D. Sindayihebura, J. Cousin and C. Dumouchel, *Part. Part. Syst. Charact.*, **14**, 93 (1997).
46. T. J. Mason, *Ultrason. Sonochem.*, **10**, 175 (2003).
47. J. Stryckers, T. Swusten, W. Brullot, J. D'Haen, T. Verbiest and W. Deferme, *Adv. Eng. Mater.*, **20**, 1800681 (2018).
48. M. Lalo, *Atomisation d'un film liquide mince par action combinée des instabilités de Kelvin-Helmholtz et de Faraday: application aux injecteurs aérodynamiques des turbomachines aéoronautique*, Doctoral Thesis, ENSAE-ONERA, Toulouse (2006).
49. Y. Kuang, C. Guangwen, S. Lei, Y. Xiang, L. Zhang and C. Jianfeng, *Chin. J. Chem. Eng.*, **17**, 546 (2009).
50. R. J. Lang, *J. Acoust. Soc. Am.*, **34**, 6 (1962).
51. H.-J. Yang, G.-W. Chu, J.-W. Zhang, Z.-G. Shen and J.-F. Chen, *Ind. Eng. Chem. Res.*, **44**, 7730 (2005).
52. X. Guo, Y. Fan and L. Luo, *Chem. Eng. J.*, **227**, 116 (2013).
53. F. Parvizian, M. Rahimi and N. Azimi, *Chem. Eng. Process.: Process Intensif.*, **57**, 8 (2012).
54. N. Aoki, T. Fukuda, N. Maeda and K. Mae, *Chem. Eng. J.*, **227**,

198 (2013).
55. L. Gaete-Garretón, D. Briceño-Gutiérrez, Y. Vargas-Hernández and C. Zanelli, *J. Acoust. Soc. Am*., **144**, 222 (2018).
56. D.-Y. Kang and J.-H. Kim, *Korean J. Chem. Eng*., **38**, 2286 (2021).
57. J. C. Simon, O. A. Sapozhnikov, V. A. Khokhlova, L. A. Crum and M. R. Bailey, *J. Fluid Mech*., **766**, 129 (2015).
58. L. Zhang, C. Srinivasakannan, S. Li, Y. He, K. Chen and S. Yin, *Microchem. J*., **155**, 104662 (2020).
59. S. Ferrouillat, P. Tochon and H. Peerhossaini, *Chem. Eng. Process.: Process Intensif*., **45**, 633 (2006).